A RUBIDIUM CLOCK FOR GPS

William J. Riley
EG&G, Inc., Frequency and Time Department
Salem, Massachusetts

ABSTRACT

The work at EG&G, Inc. on a second-source rubidium frequency standard for use in the GPS navigation satellites has now reached the prototype stage. This paper describes (1) the design objectives and approach, (2) the more important design features, (3) the signal parameters and error budget, and (4) the early results of this program up to the present.

INTRODUCTION

Since March 1980, EG&G, Inc., has been engaged in a program to develop a rubidium frequency standard (RFS) for the Department of Defense, NAVSTAR Global Positioning System (GPS). This paper describes the RFS design objectives and approach as well as the early test results obtained up to the present prototype stage of development.

The basic objective in the RFS development is to meet the stringent stability, reliability, and radiation hardness requirements of the Phase III NAVSTAR satellites. A summary of the general specifications is contained in Table 1.* The overall design approach has been to choose a configuration that favors the highest possible performance and, wherever possible, uses mature S-level quality parts. All parts will be subjected to extensive screening.

The design objective of radiation hardness will be met by circuit design, component selection, and passive shielding.

To ensure the highest possible performance, the design utilizes a discrete filter cell arrangement to permit separate control of the optical pumping spectrum. This allows the light shift effect to be independently nulled and reduces inhomogeneities in the absorption cell.

---

*Tables are located at the end of the paper.

The synthesizer is based on a 10.23 MHz output and uses a direct primary loop multiplier chain for high spectral purity. The physics package makes effective use of the vacuum environment for thermal insulation, thus reducing oven operating power.

The early results obtained during the prototype development are encouraging, and the unit uses less than half the power than the original GPS rubidium clock (12 versus 28 watts), although it is somewhat larger (260 versus 170 cubic inches) and heavier (10.5 including radiation shielding versus 9.7 pounds). The weight factor has only recently increased in importance, and a weight reduction effort is currently underway.

It is expected that one of the prototype units will be subjected to extended stability testing, which will be followed by the building and testing of qualification units. This program should result in the production of the most stable rubidium clocks yet manufactured.

SYSTEM BLOCK DIAGRAM

A block diagram of the complete RFS system is shown in Figure 1. The major sections, which are discussed separately on the following pages, are listed below:

(1) The physics package that serves as a frequency discriminator by generating an error signal whose magnitude and sense indicates the difference in frequency between the microwave excitation and the stable atomic resonance.

(2) The supporting electronics that allow proper operation of the physics package.

(3) The primary loop that produces an output signal whose frequency is locked to an exact submultiple of the atomic resonance.

(4) The secondary loop that synthesizes the desired 10.23 MHz output.

(5) The control circuits that allow remote tuning, mode selection, and monitoring.

(6) The power supply.

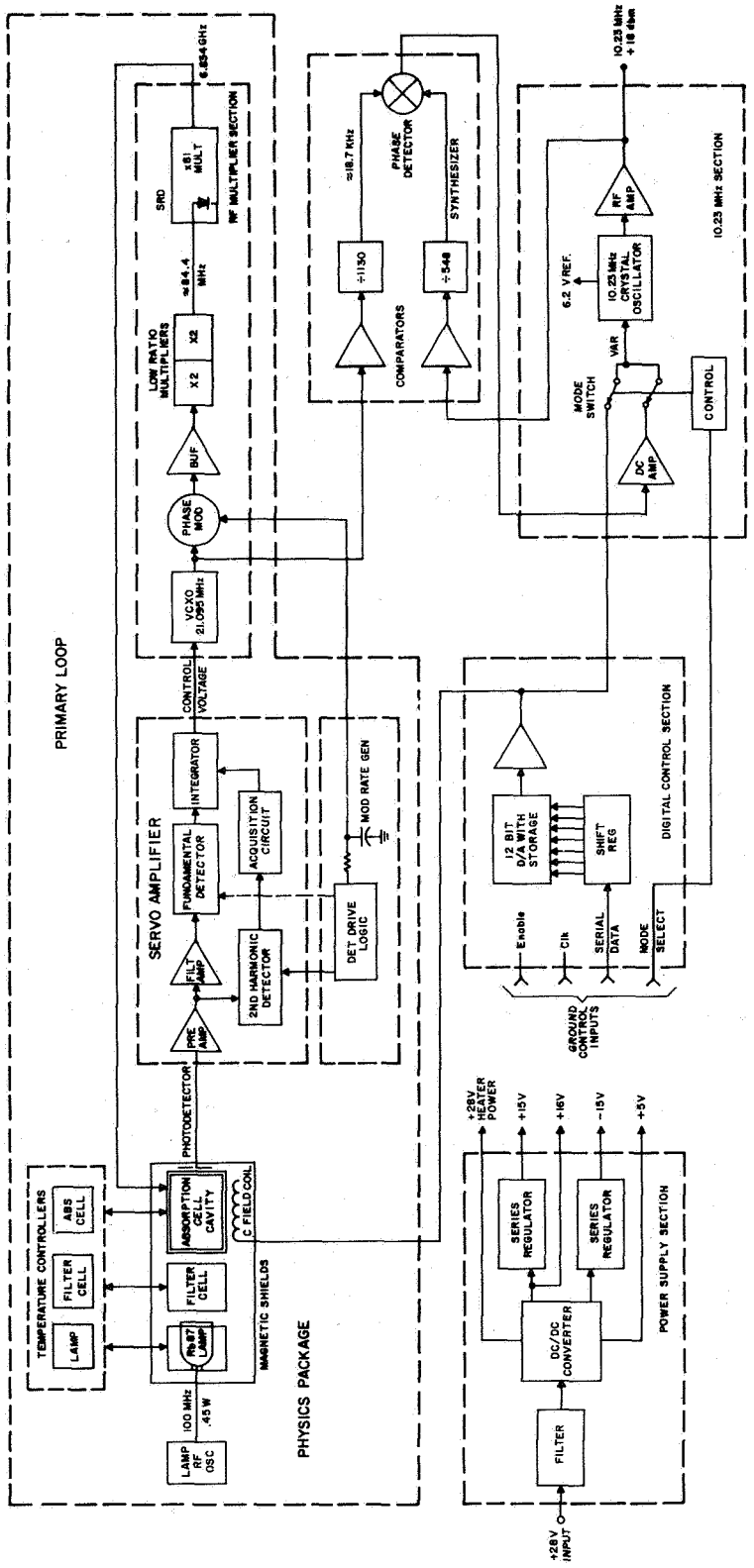

Figure 1 – GPS RFS system block diagram

Physics Package

The physics package design is based on classical rubidium frequency standard principles, except for the use of a smaller TE_{111} cavity. This approach gives the highest performance consistent with allowable size. The discrete filter cell gives zero light shift (ZLS) over a range of light intensity and a high S/N ratio. This permits operation at a relatively low light level, thus reducing temperature and rf power dependencies.

The characteristics of the lamp, filter, and absorption cell are shown in Table 2. The lamp operates in the Kr-Rb mixed mode and is excited with 0.45 watt of rf power at 110 MHz. The lamp D_1 line emission at 794.7 nm is shown in Figure 2a; it is free of self-reversal. Lamp life is aided by tight heat sinking, alkali resistant glass, high vacuum processing, and calorimetric measurement of rubidium fill.

An example of calorimetric measurement is shown in Figure 3. A differential scanning calorimeter, Perkin-Elmer DSC-2C, is used to measure the heat energy required to melt the rubidium in a lamp. This allows (using the known heat of fusion of Rb) the amount of rubidium to be determined with a resolution of a few μG. A test program is underway to evaluate lamp life using this technique.

The filter cell is operated in a separate oven whose temperature is adjusted for ZLS. The spectrum of the filtered light is shown in Figure 2b. Notice that ZLS filtration corresponds to only a slight attenuation of the skirt of the unwanted hyperfine optical component. Heavier filtration with a longer or hotter isotopic filter gives a stronger signal and lower filter cell TC but only at the expense of a large negative light shift coefficient. The filter cell buffer gas and pressure were chosen to give optimum signal and lowest TC under ZLS conditions.

The absorption cell buffer gases are chosen for narrow linewidth and low TC. The mix ratio is adjusted for a slightly positive TC to partially compensate for the filter cell TC. The nominal fill pressure is determined by the synthesizer ratio and is sufficient to reduce the wall relaxation rate without excessive buffer gas collisional broadening. The absorption cell length is optimized for maximum signal at the chosen light intensity and temperature, the latter being the coolest practical value for the required upper ambient limit of 45°C.

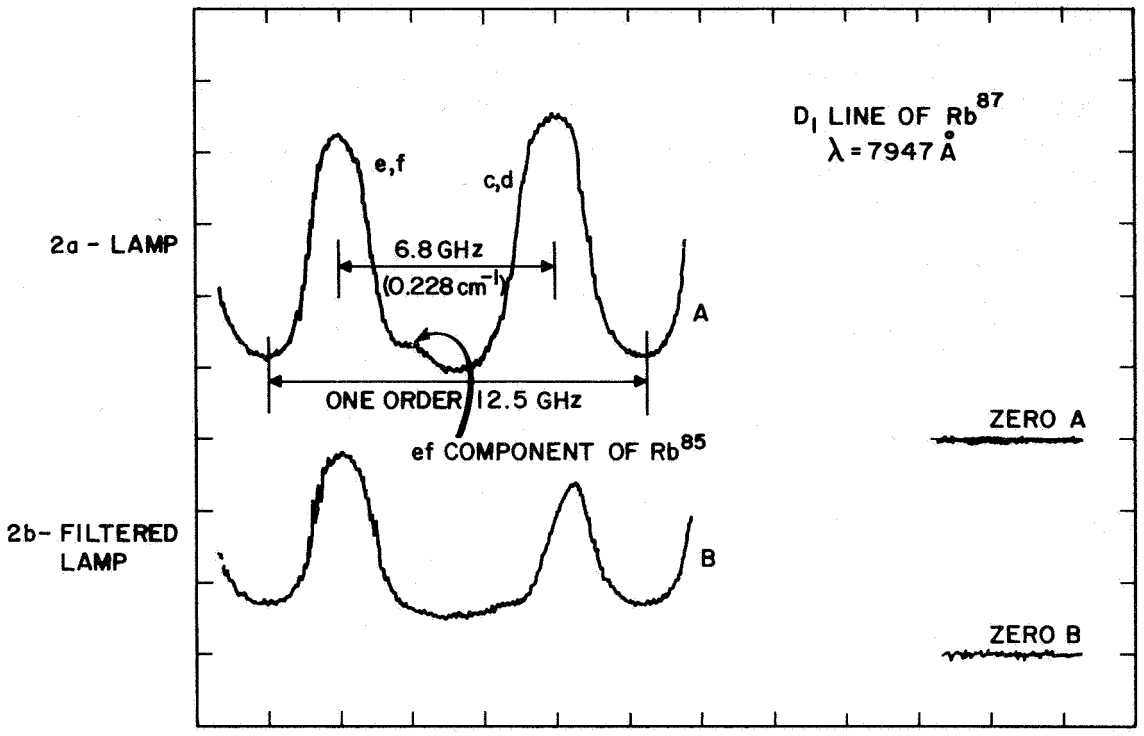

Figure 2 — Hyperfine light spectra

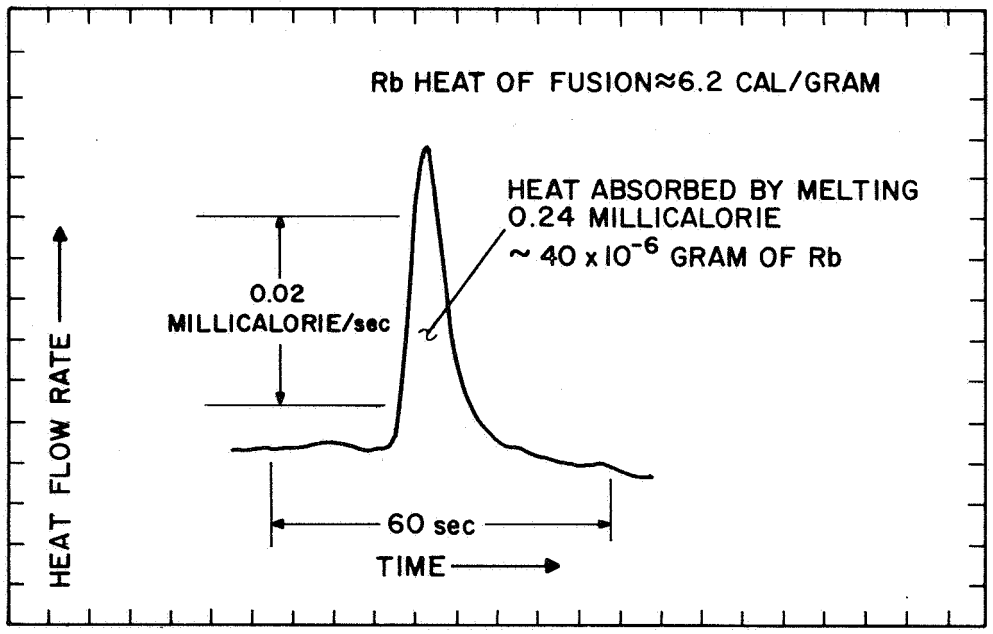

Figure 3 — Rb determination by calorimetry

A cross-sectional view of the physics package is shown in Figure 4. The three ovens are supported by a fiberglass structure with finger-like tabs that combine rigidity with low thermal conductance. This makes effective use of the vacuum environment for thermal insulation. Low thermal conductivity leads and low emissivity gold foil further reduce losses so that the entire physics package requires only 1.8 watts of oven power under nominal operating conditions.

It is important to avoid any condition that can distort the shape of the absorption line, because any such inhomogeneity will contribute to the rf power dependence. A lens is used to collimate the lamp output and provide a uniform light distribution, the filter cell is adjusted for ZLS, a two-section C-field coil configuration provides a uniform magnetic bias field, and a well bonded absorption cell with modest pressure shift coefficient provides low temperature gradients. All oven windows are sapphire for high thermal conductivity.

Another consideration is the residual magnetic field of the oven heaters which, particularly for the cavity, can induce a pseudo temperature coefficient. Precise registration of a thin double-layer blanket heater and low oven supply current reduce this effect to 2 μG/mA or 2 x 10^{-14}/°C.

The microwave cavity is excited with an E-probe and has slotted end covers that support the desired TE_{111} mode while allowing light transmission without significant microwave leakage.

The physics package includes two 0.025 inch Hipernom cylindrical magnetic shields. The major physics package parts are shown in Figure 5.

Supporting Electronics

Directly associated with the physics package are the temperature controllers, lamp exciter, photodetector preamplifier, and magnetic bias current supply. These circuits determine, to a large extent, the overall frequency stability that is achieved.

The temperature controllers (Figure 6) are dc thermistor bridges and dissipative regulators, with static thermal gains of about 2000. The oven demand power is determined by the one hour warmup required for ground testing in air. Vacuum conditions not only reduce the oven losses but also raise the thermal gains and servo stability margins. Care is taken to hold thermistor self-heating constant at a fraction of a degree C.

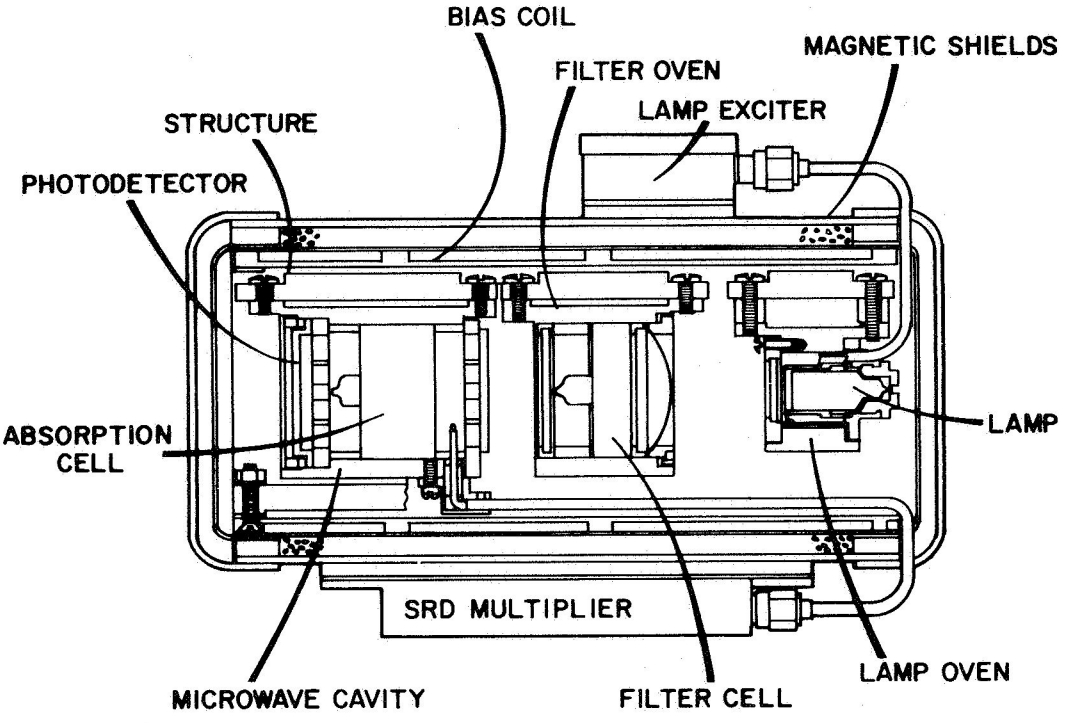

Figure 4 — Breadboard physics package cross-sectional drawing

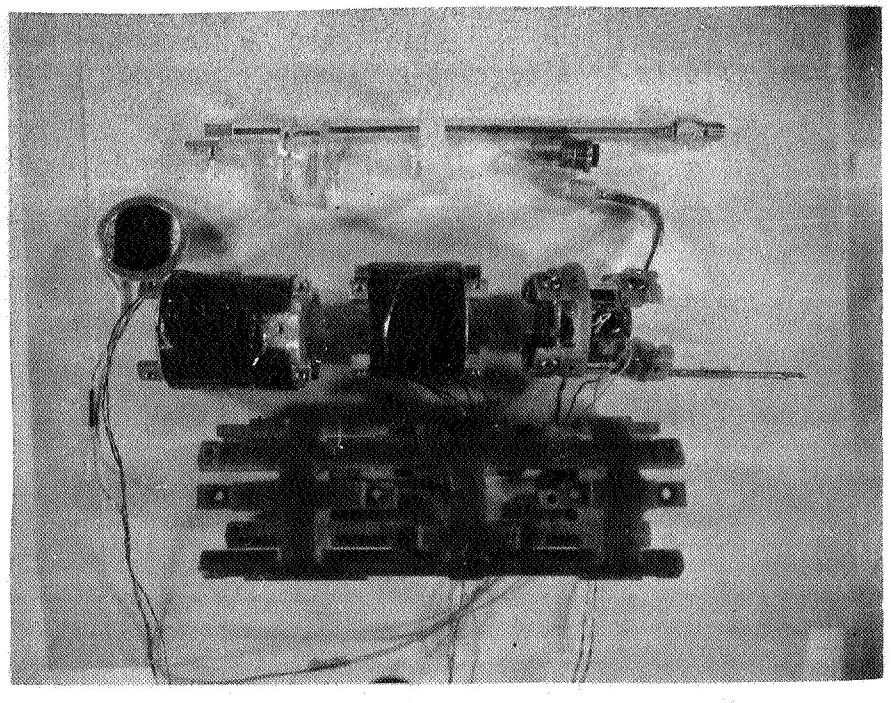

Figure 5 — Breadboard physics package parts

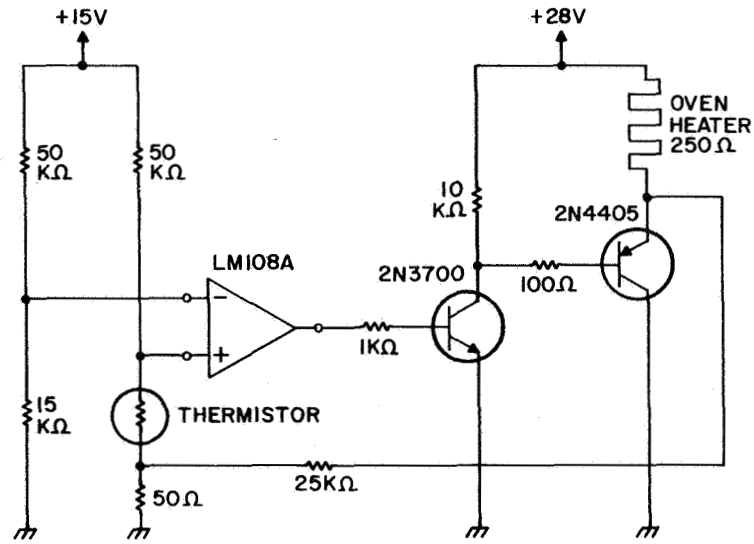

Figure 6 — Basic temperature controller circuit

The lamp exciter (Figure 7) is a straightforward Clapp power oscillator with the lamp located inside the series-tuned coil. The lamp network presents a range of loads as a function of lamp mode, and the circuit has been characterized under these various conditions to ensure proper operation. Starting may require the exciter to redistribute condensed rubidium inside the lamp by rf induction heating. Ignition takes place when sufficient voltage exists across the lamp coil. The running condition is stabilized against environmental changes and supply ripple by a current regulator circuit.

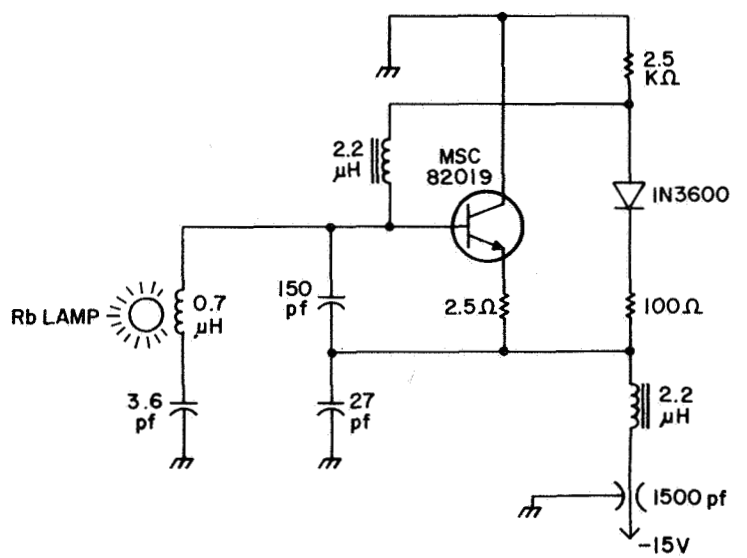

Figure 7 — Basic lamp exciter circuit

The photodetector preamplifier (Figure 8) is a two-stage configuration with dc and ac transimpedances of 100 kΩ and 5 MΩ, respectively. The ac gain is broadly peaked at the fundamental modulation frequency.

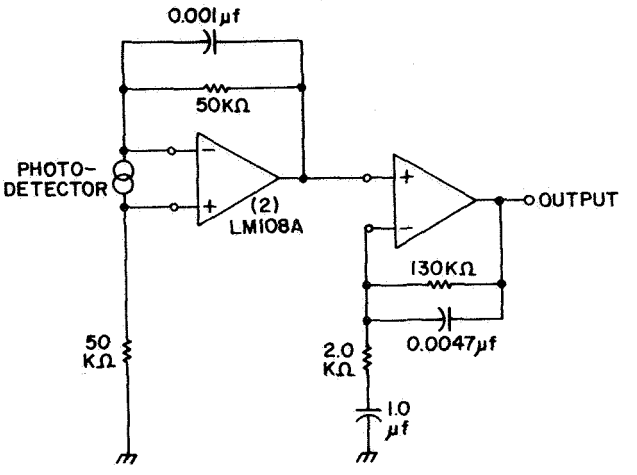

Figure 8 — Basic preamplifier circuit

The magnetic bias supply (Figure 9) is an active current source, programmable under ground control with a resolution of 3 x 10^{-12}. Relay switched fixed resistors are used for the four most significant of 12 bits, in order to minimize temperature effects on this critical circuit. The reference voltage for the C-field supply is derived from a precision zener diode located inside the oven of the secondary loop crystal oscillator. Provision is made for the direct use of this oscillator in a backup mode independent of the rubidium reference.

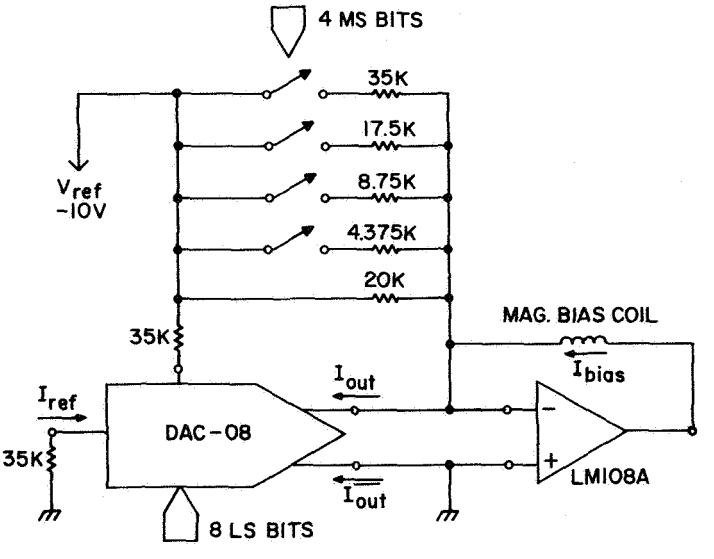

Figure 9 — Basic magnetic bias supply circuit

Primary Loop Electronics

The servo amplifier, crystal oscillator, and rf multiplier chain that complete the primary loop are shown in Figure 10. No synthesis or mixing is done in this loop to avoid instability caused by asymmetrical components on the microwave spectrum. The amount of frequency offset caused by a single spurious component scales directly with its power and inversely with its separation from the main carrier. A typical sensitivity is 5×10^{-13} for a component equal in power and 5 MHz away. Direct multiplication essentially eliminates this effect. The most critical components are at ±18.7 kHz (from the secondary loop synthesizer) that are well suppressed (>-60 dBC) and symmetrical.

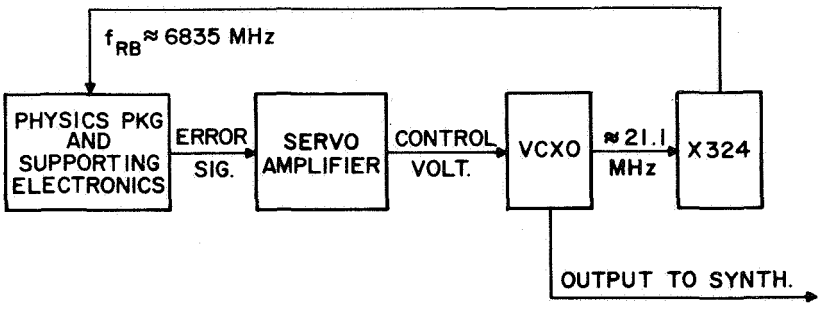

Figure 10 — Primary loop block diagram

The servo amplifier (Figure 11) consists of a main fundamental detector/integrator channel, a second harmonic/acquisition channel, and the modulation reference logic. The modulation rate is derived by division of the 10.23 MHz output to approximately 146 Hz. The servo amplifier circuits, although straightforward, require care in execution and component selection, since the system is a frequency lock loop and offsets directly cause frequency errors.

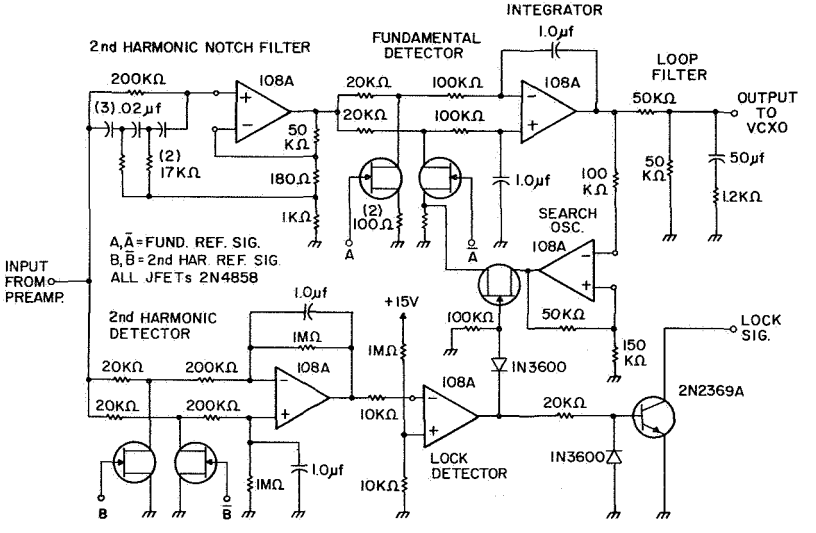

Figure 11 — Basic servo amplifier circuit

The crystal oscillator (made by Frequency Electronics, Inc.) uses an FC-type crystal which, by virtue of its excellent temperature characteristic, avoids the need for ovenization.

The rf multiplier chain (Figure 12) consists of a phase modulator, two push-push doublers, and a X81 step recovery diode (SRD) multiplier. An ALC loop is used to maintain constant drive to the SRD multiplier. This approach gives high stability and spectral purity with minimum complexity. Particular care is taken to avoid frequency offsets caused by even-order modulation distortion. A relative second harmonic distortion level of -70 dB can cause an offset of 5×10^{-12} and thus must be constant to a few percent to obtain good frequency stability. A pure modulation waveform is generated by passive integration of a precision squarewave, and a highly linear phase modulator characteristic is obtained by applying small excursions to a hyperabrupt varactor diode biased at an "S" shaped inflection point. A more subtle factor is the distortion caused by AM and subsequent AM-to-PM conversion in the multiplier chain. A simple RC phase shifter circuit introduces equal amounts of AM and PM and thus can cause considerable distortion. The all-pass phase modulator configuration shown in Figure 12 provides about 26 dB of AM rejection and thus greatly reduces this problem.

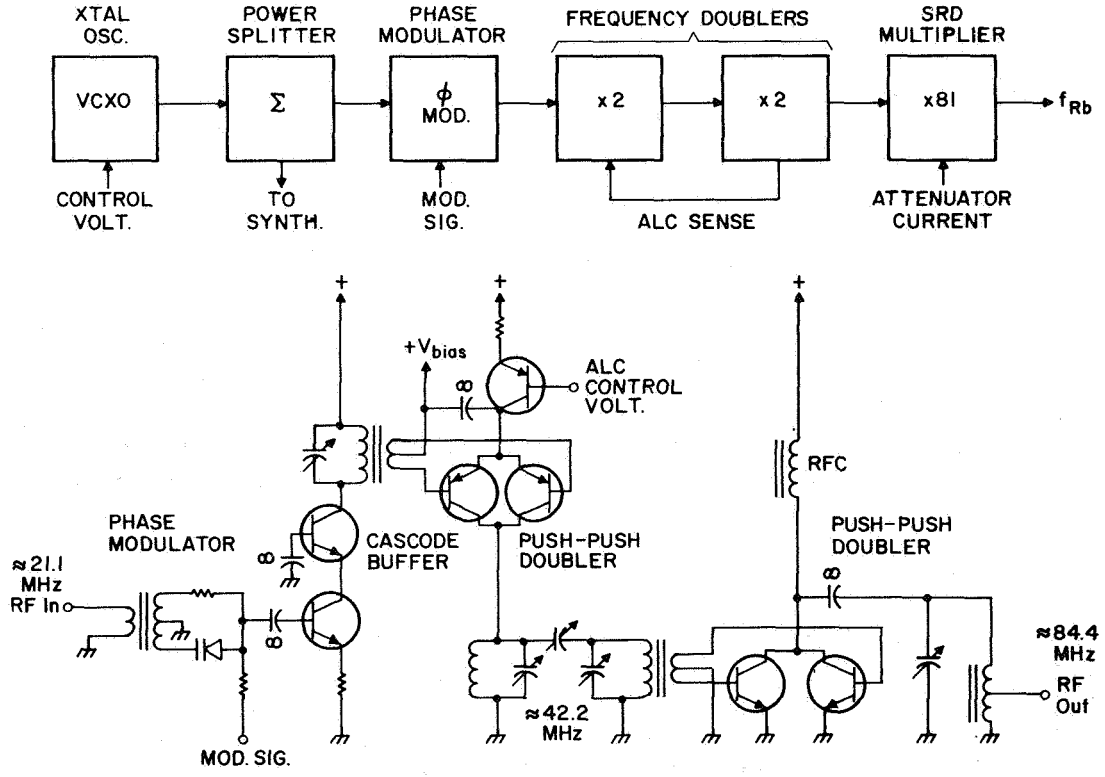

Figure 12 – Basic rf multiplier chain and circuit

The SRD multiplier (made by Frequency Sources, Inc.) uses a low capacitance diode in a shunt mode with external dc bias. A temperature stability of 0.01 dB/°C is typical for the ≈50 μW microwave output which can be adjusted to the optimum level by an internal PIN diode attenuator.

Secondary Loop and Synthesizer

The 10.23 MHz output is derived from a precision ovenized crystal oscillator (made by Frequency Electronics, Inc.) that is phase locked to the primary loop by the synthesizer. (See Figure 13.) The +18 dBm output is obtained via an output amplifier that has sufficient tank circuit Q to maintain a phase-continuous output under transient radiation. Sufficient isolation is provided by the divider input circuits to keep the output spectrum free (-100 dBC) of synthesizer spurii.

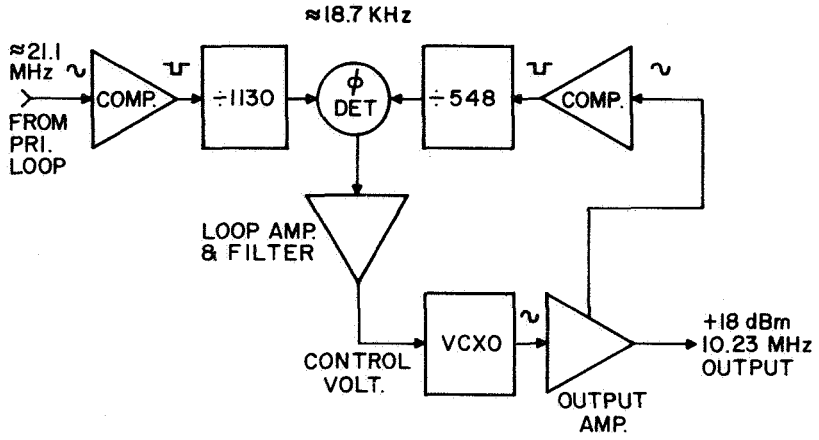

Figure 13 — Synthesizer block diagram

The synthesizer consists of a pair of dividers that divide the primary and secondary loop frequencies down to their common factor of ≈ 18.7 kHz. A phase detector and loop filter generates a control voltage for the 10.23 MHz crystal oscillator. Rapid lock acquisition is accomplished by logic that presets the dividers to the proper phase relationship. This also provides fast recovery from a radiation-induced upset.

Power Supply

The power supply consists of an input filter, a dc/dc converter, and two linear regulators as shown in Figure 1. The dc/dc converter (Figure 14) uses a single-ended flyback configuration that provides both dc isolation and regulation. Its +28 V and +5 V outputs are used directly as heater and logic supplies respectively while the ±16 V outputs are further stabilized by precision linear regulators before

supplying the analog circuits. Under normal operating conditions in vacuum, the RFS circuits consume under 10 watts. The total dc input is expected to be 28 watts demand during warmup and 12 watts steady state.

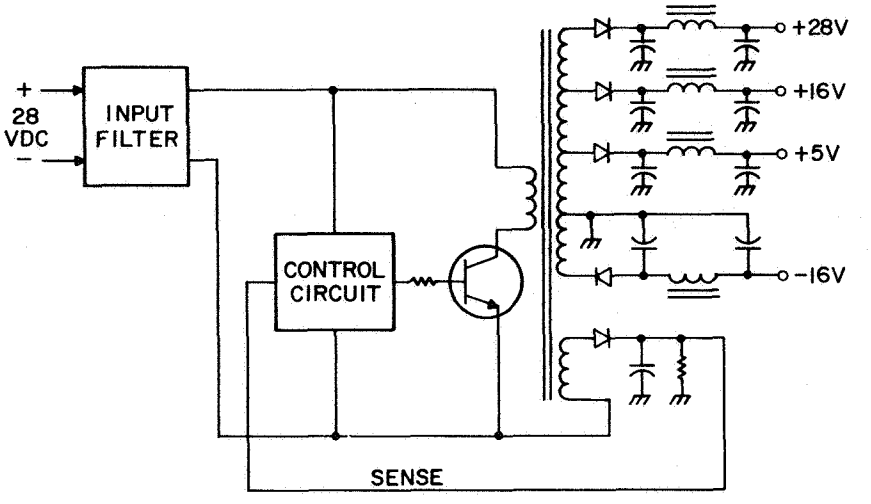

Figure 14 — Basic power supply circuit

Packaging

The overall RFS package, shown in Figure 15, consists of an aluminum structure with aluminum and Hipernom covers for magnetic, EMI, and radiation shielding. The hollow center of the structure holds the physics package, secondary crystal oscillator, the lamp exciter, preamplifier, and SRD multiplier. The other electronic circuits are on 13 circuit boards located inside compartments that comprise the outside walls of the structure. Additional local radiation shielding is used as required. This approach meets all thermal, electrical, mechanical, magnetic, and radiation requirements as well as allowing good access to most circuit boards.

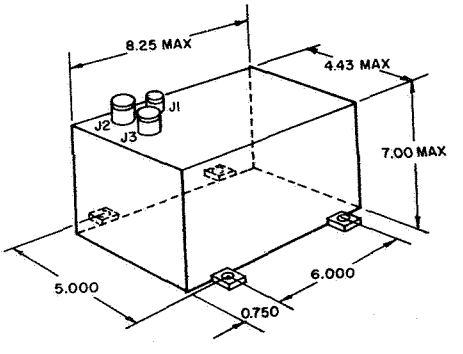

Figure 15 — RFS outline drawing

Signal Parameters

The operating conditions and signal parameters of the physics package are summarized in Table 3. In general, these values indicate a good signal and exceptionally low sensitivities.

The S/N ratio of a passive rubidium frequency standard is limited by the shot noise of the dc photodetector current, I_0, which sets a level of white frequency noise and gives a time-domain frequency stability that varies as $\tau^{-1/2}$, where τ is the averaging time.

The frequency stability can be estimated simply from the values of I_0 and the discriminator signal, D. For $I_0 \approx 82$ μA, the shot noise current, i_n, is:

$$i_n = \sqrt{2eI_0\Delta F} = 5.1 \text{ pA}/\sqrt{\text{Hz}}$$

This establishes the white frequency noise level in relation to the D value of 240 pA per 1×10^{-10}, giving a fractional frequency noise power spectral density of:

$$S_y(f) = h_0 = \left(\frac{5.1}{240} \times 10^{-10}\right)^2 = 4.5 \times 10^{-24}(\text{Hz})^{-1}$$

This results in a time-domain stability of:

$$\sigma_y(\tau) = \sqrt{\frac{h_0}{2}}\,(\tau)^{-1/2} = 1.5 \times 10^{-12}(\tau)^{-1/2}$$

which may be converted to a frequency-domain value of:

$$\mathcal{L}(f) = [\sigma_y(\tau)]^2\, \nu_0^2 \tau\, f^{-2}$$

where ν_0 is the carrier frequency of 10.23 MHz. Then,

$$\mathcal{L}(f) = 2.4 \times 10^{-10}\, f^{-2} \text{ and } \mathcal{L}(1) = -96 \text{ dBC/Hz}.$$

The measured noise level is 5.5 pA$\sqrt{\text{Hz}}$ rather than the 5.1 pA/$\sqrt{\text{Hz}}$ value expected from shot noise only. The noise level is 0.7 pA/$\sqrt{\text{Hz}}$ without light, also indicating a negligible contribution from the

photodetector and pre-amplifier. This is possible primarily because of the use of a very high quality EG&G custom photodetector that has a high leakage resistance (>50K Ω) at the 65°C operating temperature.

The actual noise results in an estimated time-domain stability of 1.6 x 10^{-12} $\tau^{-1/2}$. The observed value is 4 x 10^{-12} $\tau^{-1/2}$ uncorrected for the (unknown) contribution of the reference.

The S/N ratio can be defined as the rms value of the maximum fundamental error signal current divided by the rms noise current in a 1 Hz bandwidth.

Values of over 90 dB have been obtained with this design by operating the lamp in the more intense red (all Rb) mode, and over 80 dB in the mixed (Kr-Rb) mode. However, higher light intensity also results in larger temperature coefficients, rf power shift, and other sensitivities. For the GPS application, it is considered a better tradeoff to favor long-term and environmental stability by operating at modest light intensity where the S/N ratio is about 75 dB.

ERROR BUDGET

The RFS frequency is influenced by a number of factors that can affect its stability. Some of these factors involve dependencies of the physics package and others are a result of electronic circuit sensitivities. The largest of these factors are listed in Table 4. Also shown in Table 4 are the resulting individual temperature coefficients and the total worst-case and rms values expected. These factors also govern the aging rate and radiation sensitivity of the unit.

TEST RESULTS AND CONCLUSIONS

Tests of a breadboard version of the RFS have given encouraging results. The results of stability tests conducted on the primary loop with the physics package in a thermovac chamber and most electronic circuits on the bench in air are shown in Figure 16. The measured time-domain stability is within the goal specification. The results are uncorrected for the contribution of the reference and are probably limited by the reference stability in the medium term region. The region near τ = 1 second will be determined by the secondary loop crystal oscillator, which has a measured stability of 4 x 10^{-12}. The RFS stability in the medium term region is at least as low as 4 x 10^{-12} $\tau^{-1/2}$ and reaches below 1 x 10^{-13} between $\tau = 10^4$ and 10^5 seconds. The Rb reference is better in the medium term region, but the Cs reference has been found to be better at 10^4 seconds and longer, probably because of the barometric sensitivity of the rubidium reference unit. The GPS RFS is immune to this effect in the thermovac chamber. A drift rate of under 1 x 10^{-13} per day and a physics

package temperature coefficient of 1 x 10^{-13}/°C has been obtained. It is reasonable to assume that the 10^5 second stability will be even better in the prototype version, when all circuits are packaged and operated within the controlled thermovac environment. Overall, the RFS program is on schedule and all objectives are being met.

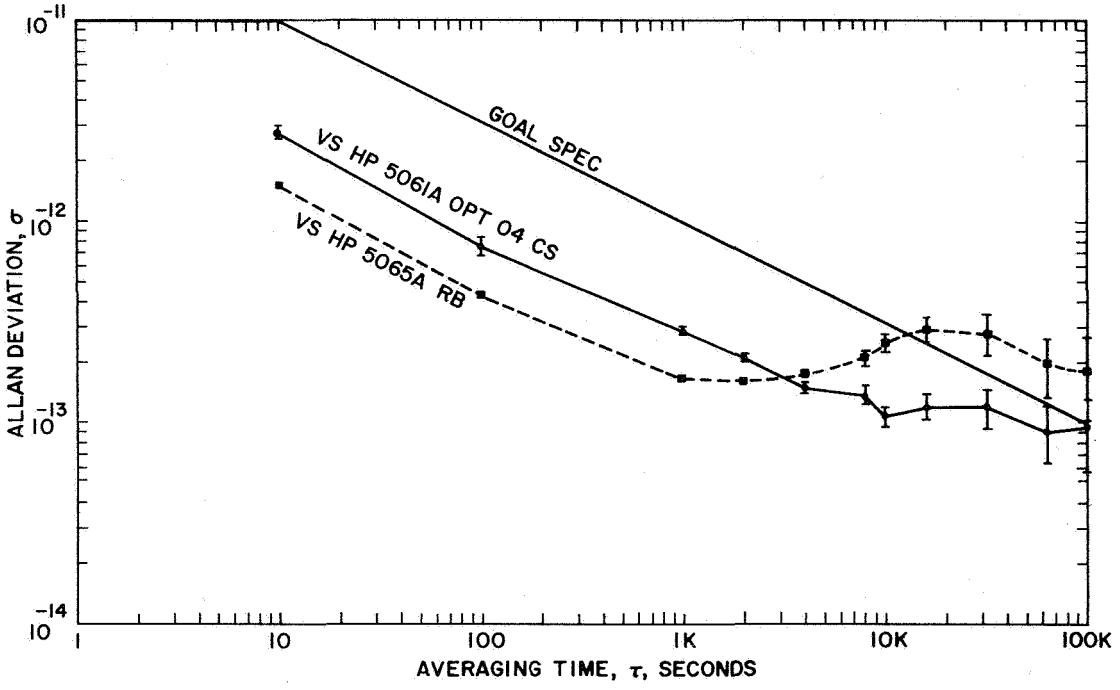

Figure 16 — Time-domain stability of the breadboard

ACKNOWLEDGMENTS

The author wishes to acknowledge the support of Rockwell International, Space Division, and the Department of the Air Force, Headquarters Space Division (AFSC), Directorate of Space Navigation Systems for their sponsorship of this work. The program has benefitted by technical advice from the Aerospace Corporation and the radiation hardening expertise of JAYCOR Inc. Also, we received valuable consultation from Professor J. Vanier of Laval University and Mr. H.P. Stratemeyer.

The work at EG&G has been a team effort and important contributions have been made by all staff members. Particular credit should be given to Mr. T. Lynch in the area of thermal-mechanical design and for the concept of calorimetric rubidium measurement; Mr. E. Sullivan for power supply and synthesizer design; and Mr. S. Goldberg for his overall scientific direction. Other design contributions were made by F. Chang, J. Kirby, K. Lyon, and J. McDonald.

Table 1 — Condensation of specifications for the Phase III GPS RFS

Output	f = 10.23 MHz nominal, +18 dBm nominal
Operating Temperature	+ 20 to +45°C
Frequency Stability (Figure 16)	$\sigma_y(\tau) = 1 \times 10^{-11}$ for τ = 1 and 10 seconds decreasing as $\sqrt{\tau}$ to goal of 1×10^{-13} at 10^5 seconds
Phase Noise	$\mathcal{L}(1)$ = -83 dBC/Hz maximum, decreasing at 10 dB/decade to 5 kHz
Spurious	-100 dBC maximum, 5 kHz to 20 MHz from carrier
Temperature Coefficient	$\frac{\Delta f}{f} \leq 1 \times 10^{-12}$/°C
Drift	$\frac{\Delta f}{f} \leq 1 \times 10^{-13}$/day
Voltage Sensitivity	$\frac{\Delta f}{f} \leq 1 \times 10^{-12}$/volt
Mag Susceptibility	$\frac{\Delta f}{f} \leq 1 \times 10^{-12}$/3 Gauss
Warmup Time	1 hour
Reliability	73% for 7.5 years' operation

Table 2 – Lamp and cell characteristics

	Lamp	Filter Cell	Absorption Cell
Glass (Corning #)	1720	7070	7070
Outside Diameter, inches	0.31	1.09	1.09
Inside Length, inches	0.54	0.18	0.45
Isotope	87	85	87
Buffer Gas	Kr	Ar	N_2/Ar = 0.731
Pressure, Torr	7	120	14.2*
Operating Temperature, °C	120	85	65
Temperature Coefficient $pp10^{11}$/°C	~0	-6	+3

*Offset = +2.78 kHz.

Table 3 — Breadboard RFS operating characteristics

Signal	
Second Harmonic Signal:	45 mV rms*
Maximum Fundamental Signal:	165 mV rms*
Light:	8.23 Vdc*
Discriminator Slope:	1.2 mV per 1×10^{-10}*
Linewidth:	252 Hz†
Sensitivities	
Light Shift:	$\sim 0 \pm 1 \times 10^{-12}$/%
Lamp Oven TC:	$\sim 0 \pm 3 \times 10^{-12}$/°C
Filter Cell TC:	$\approx - 6 \times 10^{-11}$/°C
Absorption Cell TC:	$\approx + 3 \times 10^{-11}$/°C
RF Power Shift	$\approx \pm 2 \times 10^{-12}$/dB
Lamp Exciter TC:	$\sim 0 \pm 5 \times 10^{-14}$/°C
Noise	
Shot Noise:	5.1 pA/$\sqrt{\text{Hz}}$
Total Noise:	5.5 pA/$\sqrt{\text{Hz}}$
Signal:	33 nA rms
(S/N):	76 dB in 1 Hz BW
Line Q:	16×10^6
Predicted Stability:	$\sigma_y(\tau) = 1.6 \times 10^{-12}\, \tau^{-1/2}$

*At preamp output with Z_T(ac) = 5 MΩ, Z_T(dc) = 100 KΩ.

†Full width between inflection points with normal light and rf.

Table 4 — Frequency error budget

Factor	Sensitivity	TC, pp10^{14}/°C
Magnetic Bias Current	+ 3 x 10^{-14}/ppm	± 6.0
Lamp Exciter TC	± 5 x 10^{-14}/°C	± 4.0
Filter Cell TC	- 6 x 10^{-11}/°C	- 3.0
$d\phi/dt$ Effects	---	± 2.5
RF Level Shift	± 2 x 10^{-12}/dB	± 2.0
Residual Heater Field	± 5 x 10^{-14}/mA	± 2.0
Absorption Cell TC	+ 3 x 10^{-11}/°C	+ 1.5
VCXO Dynamic TC	---	± 1.5
Servo Integrator	± 1 x 10^{-14}/°C	± 1.0
Power Supply	± 1 x 10^{-12}/%	± 1.0
Modulation Deviation	± 1 x 10^{-13}/%	± 1.0
Miscellaneous	---	± 1.0
Total		Worst-case 23.5
		rms 9.2